Smartphone as a Fluorescence Detector for High-Performance Liquid Chromatography

3

1

2

- Danial Shamsaei, Shu-An Hsieh, Iran Ocaña Rios, Saxon J. Ryan, and Jared L. Anderson, and
- 6 Department of Chemistry, Iowa State University, Ames, IA 50011 USA
- ²Department of Agricultural and Biosystems Engineering, Iowa State University, Ames, IA 50011 USA

8

9

Abstract

<u>Background</u>: Fluorescence detection is employed in high-performance liquid chromatography (HPLC) due to its high specificity and sensitivity. However, it is often limited by expensive components and bulkiness. Recently, advances in technology and electronics have led to the development of smartphones that can serve as portable recording, analysis, and monitoring tools. Smartphone-based detection provides advantages of cost effectiveness, rapid signal/data processing, and the display of results on a handhold monitor. The combination of smartphone-based detection with HPLC can offer unique features that are beneficial in overcoming limitations of commercial fluorescence detectors. (90)

Results: A miniaturized and low-cost HPLC fluorescence detector based on a smartphone is introduced for the detection of six fluorescent molecules. The smartphone is able to capture emitted fluorescence in video format while MATLAB code is used for data processing to provide chromatograms based on different detection channels. A custom designed double-channel flow cell was utilized to enable simultaneous detection of fluorescent compounds with different excitation wavelengths. The detector consists of a lab-made flow cell, monochromatic LEDs as the light source, 3D printed housing and connector box, fiber optic cables, and a smartphone. The effects of flow cell geometry, channel width and light slit diameter, as well as a comparison of different flow cell manufacturing techniques, are studied and discussed. The validated system was successfully applied to samples from diverse water sources, yielding spiking recoveries within the range of 91.7% and 109.7%. (141)

<u>Significance</u>: This study introduces the first smartphone-based fluorescence detector for HPLC with cost-effective and customizable flow cells, allowing for the simultaneous detection of fluorescent compounds with different excitation wavelengths and offering a potential solution for the analysis of co-eluting compounds. Beyond its user-friendly interface and low-cost, smartphone detection in HPLC provides tremendous opportunities in further miniaturizing

mechanisms of detection. (70) Keywords: smartphone; high-performance liquid chromatography; fluorescence detection; coumarin dyes; miniaturized detectors; 3D printing *Corresponding Author: Jared L. Anderson Department of Chemistry Iowa State University 1605 Gilman Hall Ames, IA 50011 Email: andersoj@iastate.edu

chromatographic instrumentation while offering high sensitivity and can be expanded to other

1. Introduction

35

36

37

38

39

40

41

42

43

44

45

46

47

48

49

50

51

52

53

54

55

56

Fluorescence is a form of luminescence in which molecules absorb light of a particular wavelength and emit light of longer wavelengths. In high-performance liquid chromatography (HPLC), fluorescence detectors are used to due to their high sensitivity and selectivity [1]. They are considered to be selective detectors due to the fact that their excitation and emission wavelengths are specific for a given molecule, providing them advantages over ultraviolet (UV) detectors which respond to nearly all molecules with moderate to strong chromophores [2,3]. Since fluorescence intensity is often directly proportional to the intensity of the excitation source, fluorescence detectors offer high sensitivity through the use of intense light sources. Most commercially-available detectors used in HPLC are equipped with a xenon lamp as the excitation source, sophisticated excitation and emission monochromators, optical modules, and a photomultiplier tube (PMT). However, the use of xenon lamps has certain drawbacks, including their short lifetime, low light intensity stability, high energy consumption, and high replacement costs. Additionally, the application of PMTs is limited due to their high cost and propensity of being sensitive to vibrations, electromagnetic fields, and light leakage [4,5]. Moreover, computers are generally required to control the excitation/emission wavelengths as well as the acquisition and processing of data which ultimately limits their portability. There is a growing trend within the field of chemical analysis to develop miniaturized, portable, and low-cost instrumentation [6]. Over the last several years, a number of miniaturized detectors for HPLC have been reported including the photothermal absorbance detector [7], UV absorption detector [8,9] and electrochemical detector [10]. However, a low-cost, user-friendly and miniaturized fluorescence detector for HPLC has yet to be introduced and remains as an unmet need.

To meet the goals of miniaturizing components and reducing the costs of chemical analysis, widely-available light recording and light analyzing devices such as cameras [11,12], monitor calibrators [13,14], Raspberry Pi [15,16], ocean optic [17], and smartphones [18,19] have been reported. Among these devices, smartphones have attracted extensive attention in the analytical chemistry community due to their accessibility, versatility, and compactness [20,21]. Smartphones employ fast, multi-core processors that enable them to process signals rapidly without requiring connection to a computer, while also offering other exclusive features such as a touch screen, high capacity memory for data storage, long battery lifetimes, and high quality cameras that are tolerant to ambient light, electromagnetic interference and vibration are among important features of a portable detector [22,23]. Smartphones have been applied to a number of techniques employing fluorescence [24–26], colorimetry [27–29], chemiluminescence [30–32], and electroluminescence [33] to produce reliable, low-cost, and portable spectroscopic detection methods. In recent years, the combination of smartphones with capillary electrophoresis [34], paper microfluidic cell chromatography [35] and thin layer chromatography [36] has been reported. However, the coupling of smartphones with HPLC, in particular fluorescence detection, has yet to be reported due to the following major challenges: (1) detection of fluorescence signals under the conditions of a flowing mobile phase, (2) transmission of emitted fluorescence to the smartphone for proper recording by the camera, and (3) ensuring conditions of the setup are such that the emitted fluorescence and capturing of images results in highly reproducible video recordings to maximize sensitivity.

57

58

59

60

61

62

63

64

65

66

67

68

69

70

71

72

73

74

75

76

77

78

79

In this study, we present the design and development of a smartphone-based fluorescence detector coupled to HPLC for the analysis of six fluorescent molecules. The approach involves a customized flow cell capable of withstanding high mobile phase flow rates and enabling double channel detection, LEDs as excitation sources (instead of expensive sources used in commercial fluorimeters), fiber optic cables to transfer fluorescent light to the smartphone camera for minimization of noise and signal loss, customizable 3D printed components that eliminate interference from surrounding light, detection of emitted fluorescent light using a smartphone, and MATLAB software to process and analyze recorded videos. The novel detection approach in this study utilizes a smartphone for capturing and recording the signal, thereby eliminating the need for a specialized detector while reducing the number of electronic components involved. Additionally, the system was designed based on the minimum necessary optical components by eliminating the need for optical filters, which are typically used to reduce noise and ensure emission of monochromatic light, as well as lenses used for focusing light. The optical and electrical components make the miniaturized detector low-cost and user-friendly. This study also develops a customized double-channel flow cell employing UV and green LEDs as light sources to permit the detection of two fluorescent molecules that are poorly resolved during chromatographic separation.

2. Experimental Section

2.1 Materials, standards, and instrumentation

The six studied fluorescent molecules consisted of five coumarin dyes and rhodamine B dye. Coumarin 6 (98%), coumarin 153 (99%), coumarin 120 (99%), and rhodamine B (95%) were purchased from Sigma-Aldrich (St. Louis, MO, USA). Coumarin 307 (98%) and coumarin 466 (98%) were obtained from Santa Cruz Biotechnology (Dallas, TX, USA). Acetonitrile (HPLC grade, \geq 99%), methanol (HPLC grade, \geq 99%) and chloroform (98%) were obtained from Sigma-Aldrich. Deionized water (18.2 M Ω cm) was produced by a Milli-Q water filtration system (Millipore, Bedford, MA, USA). Coumarin 6 (500 mg L⁻¹) was prepared in a methanol:acetonitrile

solution (50:50, v/v) and all other analytes (500 mg L⁻¹) were prepared in methanol in light-resistant containers and stored at 4 °C. Standard solutions were prepared daily by diluting the stock solutions in methanol.

Transparent polylactic acid (PLA), black PLA and white acrylonitrile butadiene styrene (ABS) filaments, obtained from Dynamism (Chicago, IL, USA), were used for 3D printing by an Ultimaker S5 printer (Utrecht, the Netherlands). Clear (RS-F2-GPCL-04) and black resin (RS-F2-GPBK-04), purchased from Formlabs (Somerville, MA, USA), were printed by a Form3 stereolithography printer purchased from Formlabs. Clear and black poly(methylmethacrylate) (PMMA) sheets purchased from Grainger (Clifton, NJ, USA) were cut using a Super Mini Mill machine from HAAS (Oxnard, CA, USA). Absorption spectra of all fluorescent molecules were detected with a Varian Cary 100 Bio Spectrophotometer (Palo Alto, CA, USA).

2.2 Design of single and dual-channel flow cells

Fluorescence detectors commonly used in HPLC are equipped with a xenon lamp as an excitation source and selection of the excitation wavelength of monochromatic light is carried out between the lamp and flow cell. However, these systems are bulky, expensive, and can complicate detector miniaturization. Thus, low-cost monochromatic LEDs were used in this study to enable miniaturization of the detector. A disadvantage of monochromatic LEDs is their emission of light within a narrow wavelength range (~60 nm) which limits their effectiveness in detecting analytes with similar excitation wavelengths. To overcome this limitation, monochromatic LEDs providing a desired range of wavelengths in each HPLC run were employed; however, applying several monochromatic LEDs required customization of the flow cell. Thus, in an effort to maximize customizability as well as reduce the cost of the fluorescence detector, lab-made flow cells were designed and fabricated using a computer numerical control (CNC) machine. The customizability

of CNC milling provides flexibility by enabling different designs to be imparted into the detection system. Figure 1 shows a schematic of the lab made flow cell, LED holder, and light slit that was designed and 3D printed for this study. A single-channel flow cell was developed to detect fluorescent molecules using a single LED, and a double-channel flow cell was fabricated for the detection of fluorescent molecules requiring two different wavelength ranges. The double-channel design consisted of a continuous pathway that directs eluent through channels equipped with different monochromic LEDs, as shown in Figure 2 (b). Emitted fluorescent from each channel is captured as a video that is simultaneously recorded by the smartphone camera. This innovative design significantly increases the selectivity by enabling the use of LEDs that emit light corresponding to the excitation wavelength range of a particular fluorescent molecule.

2.3 Flow cell fabrication

Two fabrication methods—3D printing and CNC milling—were assessed for construction of the flow cells. Flow cells were examined based on their compatibility with different solvents commonly employed in HPLC, as well as considering their transparence for spectroscopic analysis. To evaluate material stability, a donut-shaped design was manufactured using commercially-available materials through 3D printing and CNC milling, and subsequently subjected to various combinations of solvents. For optical characterization studies, samples of transparent PLA and clear resin measuring 5 cm in length, 5 cm in width, and 5 mm in thickness were printed, while clear PMMA was milled by a CNC machine. Transmittance spectra of the samples were recorded from 200–800 nm using a Varian Cary 100 Bio Spectrophotometer. Transparency was determined by calculating the transmittance values at 375 nm and 570 nm, which were used in this study for excitation of the fluorescent molecules.

The single and double-channel flow cells, housing, and connector box used in this work (Figures 1 and 2) were designed by SOLIDWORKS 2022 Education Edition, developed by Dassault Systèmes (Vélizy-Villacoublay, France). Each flow cell consisted of one top and bottom layer. For flow cell fabrication, channels were milled on the surface of 5 mm clear PMMA using a CNC machine. Flow cells with different channel widths and a constant channel depth of 1.4 mm were constructed. After milling channel patterns and cutting holes within the top layer, the two layers were bonded together with chloroform. To direct eluent from the HPLC column to the flow cell, PEEK tubing (0.3 mm inner diameter) from Cole-Parmer (Vernon Hills, IL, USA) was used. Collection of fluorescence emitted by the fluorescent molecules was accomplished using a fiber optic cable purchased from Thorlabs (Newton, NJ, USA) featuring an inner core diameter of 1500 μm that was attached to the flow cell, as shown in Figure 1a. The emitted fluorescence image was directed to the camera of a Samsung Galaxy S20 smartphone (Suwon-si, South Korea) by connecting the other end of the fiber optic cable to the connector, as illustrated in Figure 2 (a,b). A second fiber optic cable was added to the double-channel flow cell to direct emitted light from the second channel to the connector and smartphone, as represented in Figure 2 (c).

2.4 Setup of detection system

148

149

150

151

152

153

154

155

156

157

158

159

160

161

162

163

164

165

166

167

168

169

170

With exception of the flow cell, which was milled using CNC, all other detector components such as the housing, LED holder, light slit plate and connector box were all fabricated by 3D printing and subsequently assembled as shown in Figure 2 (a,b). Depending on whether a single-channel or double-channel design was used, either one LED or two LEDs were employed as the excitation light source. These LEDs were housed within the LED holder, as this design permits easy replacement of the appropriate LED depending excitation characteristics of the targeted analytes. In this study, two LEDs ($375 \pm 20 \text{ nm}$ and $570 \pm 30 \text{ nm}$) were obtained from

Thorlabs and Mouser Electronics (Mansfield, TX, USA), respectively, to enable detection of the coumarin and rhodamine B dyes, respectively. The light slit plate was placed between the flow cell and LED holder to control the amount of light that reaches the flow cell as well as to minimize chromatographic band broadening. Since the emission intensity of the LED depends on the applied voltage, constant voltage was applied to each LED using a Jesverty adjustable direct current power supply obtained from Amazon (Seattle, WA, USA).

2.5 Experimental design for characterization of detector performance

Fluorescence profiles of the examined analytes were obtained to develop a double-channel flow cell for detection of two analytes having similar chromatographic retention times. A single-channel design was first examined to optimize channel width and light slit diameter and these optimized parameters were then incorporated into the double-channel design.

To optimize channel width and light slit diameter, a mixture of five coumarin dyes consisting of coumarin 120 (1.0 mg L⁻¹), coumarin 466 (1.5 mg L⁻¹), coumarin 307 (2.0 mg L⁻¹), coumarin 153 (6.0 mg L⁻¹) and coumarin 6 (3.0 mg L⁻¹) were selected since they can be readily separated using reverse phase HPLC. To test the performance of the double-channel flow cell, four mixtures containing different combinations of coumarin 120 (1.5 mg L⁻¹), coumarin 466 (2.0 mg L⁻¹), coumarin 307 (1.5 mg L⁻¹), coumarin 153 (6.0 mg L⁻¹), coumarin 6 (4.5 mg L⁻¹) and rhodamine B (20.0 mg L⁻¹) were prepared. The first solution was a mixture consisting of coumarin 120, coumarin 466, coumarin 153 and coumarin 6, while the second solution consisted only of rhodamine B. The third solution was a mixture consisting of coumarin 120, coumarin 466, coumarin 153, coumarin 6, and rhodamine B. These three solutions were used to investigate the feasibility of simultaneous fluorescence detection using different excitation wavelengths within the double-channel flow cell design. The fourth solution consisted of coumarin 120, coumarin 466,

coumarin 307, coumarin 153, coumarin 6, and rhodamine B and was used to perform positive peak identification.

Chromatographic separations were carried out on a Shimadzu LC-20A HPLC (Tokyo, Japan) with a Rheodyne manual injector featuring a 20 µL sample loop. Separations were performed using a Restek Ultra C18 analytical column (250 mm x 4.6 mm i.d., 5 µm particle size) obtained from Restek Corporation (Bellefonte, PA, USA) at room temperature under isocratic mode using a methanol:water (90:10, v/v) mobile phase with a constant flow rate of 1 mL min⁻¹. As shown in the Figure S2, the eluent was first directed through a UV detector set at detection wavelengths of 235 nm and 260 nm and then entered the lab-made flow cell equipped with smartphone detection and finally to waste.

2.6 Video recording and data processing

The smartphone was set to record videos using the rear-facing camera when the standard solution was injected into the HPLC. The procedures used for video recording are provided in Supporting Information as well as in Figure S1 in the Supporting Information. All videos were processed using a customized MATLAB script. Upon opening the video in MATLAB, a region of interest (ROI) was selected. MATLAB code provided three chromatograms based on red, green, and blue (RGB) values versus time, as shown in Figure 3, by averaging the RGB values of each pixel captured from the selected ROI for each frame of the video. By manually selecting the peaks, MATLAB code calculated the area, height, width, and retention time of the peaks from the chromatograms. As observed in Figure 3a, the signal intensity for each peak was not equal in the three chromatograms. Since the peak intensity in each chromatogram depends on the maximum emission wavelength of the particular dye molecules, longer wavelengths produced higher intensities for R and G values in the chromatograms. For optimization purposes and for

construction of calibration curves, the R value was used to determine the peak area of rhodamine B, the B values were used for peak areas of coumarin 120 and coumarin 466, and the G values were used for peak areas of coumarin 307, coumarin 153, and coumarin 6. Two representative videos demonstrating the ROI detected when a band of fluorescent molecules is passed through the channel and subsequent processing of the ROI by MATLAB into the individual chromatograms are provided in the supplementary information.

2.7. Real samples

Environmental water samples were collected in Ames, IA from two lakes and one river to analyze the presence of fluorescent molecules and investigate the influence of matrix on the detection method. All samples were filtered prior to analysis. Since certain coumarin dyes exhibit low solubility in water and to ensure the solubility of all analytes while spiking at the two concentration levels, the water samples were appropriately diluted with acetonitrile.

3. Results and Discussion

3.1 Design and fabrication of detection system

The housing and connector box, shown in Figure 2, were designed and 3D printed using black PLA filament. The connector box functioned to not only isolate the smartphone camera from surrounding light but also fixed the distance and angle of the camera with respect to the end of the fiber optic cable. The distance between the smartphone and the recorded object is essential, as it can affect the signal intensity and quality of the recorded video [30]. Connector boxes with varied lengths between the camera and the end of the fiber optic cable were examined. Due to the camera lens's focal length, it was not able to clearly focus on an object at distances less than 7.5 cm. On the other hand, distances greater than 7.5 cm resulted in decreased signal by reducing the amount

of emitted light that reaches the camera. Thus, 7.5 cm was selected as an optimal distance between the camera and end of the fiber optic cable and was incorporated into the final design of the connector box. The housing was designed to accommodate the flow cell, slit plate, LED and LED holder, and also prevented light from the surroundings to enter the fiber optic cable and flow cell.

3.2 Solvent compatibility and optical transparency of the flow cell

Flow cells used for fluorescence studies in HPLC are exposed to a wide variety of solvent combinations [37]. Therefore, it is important to identify materials that are compatible with the mobile phase composition for construction of the flow cell. Four types of commercially-available 3D printing materials and two types of PMMA were examined by preparing a model using the aforementioned procedure. The models were then exposed to different solvents and solvent combinations for 10 hours followed by measuring the percent change in mass. Materials that exhibited minimal swelling and softening offered the highest solvent compatibility. As shown in Table S1, all materials exhibited good compatibility with water whereas ABS and clear PMMA exhibited the best compatibility with methanol. The model created from clear resin provided the smallest change in mass when exposed to acetonitrile and its combinations; however, the observed change in mass was larger than the mass change for ABS and clear PMMA when they were exposed to methanol.

Optical transparency of the flow cell is an additional characteristic that needs to be examined to assess the efficiency of transmitting light from the LEDs to the fluorescent molecules. As shown in Figure S3a, the transparency of 3D printed models and CNC-machined parts was evaluated by collecting transmittance spectra from 200–800 nm. All experiments were performed using three different samples of printed and milled components. For clear PMMA, the transmittance exceeded 90% within the 400 nm to 800 nm range, while a transmittance of over

60% was observed up to 300 nm. Beyond 300 nm, a notable reduction in clear PMMA transmittance was observed. In the case of the 3D printed samples, transmittance in the entire UV-Vis range for the clear resin and transparent PLA fell to below 15% and 0.6%, respectively. Additionally, the transmittance values at 375 nm (T_{375nm}) and 570 nm (T_{570nm}) for all samples were measured and are represented in Figure S3b. Although it is more convenient to manufacture flow cells using 3D printing, the flow cell is less transparent compared to using clear PMMA by CNC milling and requires more optical components to transfer light into the channel(s). Therefore, clear PMMA was chosen for construction of the flow cell using a CNC mill, and a mobile phase composed of methanol and water was used throughout the study.

To assess the impact of methanol exposure on the transparency of clear PMMA, samples of clear PMMA were exposed to methanol for seven days followed by measurement of their transparency. The results demonstrated that the average of T_{375nm} and T_{570nm} values changed by less than 0.5%. To ascertain whether there is significant differences in T_{375nm} and T_{570nm} values between the PMMA samples exposed to methanol and untreated PMMA samples, a Student's t-test was performed at a significance level of 0.05 for a two-tailed distribution. The calculated p-values for T_{375nm} and T_{570nm} are presented in Table S2. The p-values suggest that there is no significant difference in T_{375nm} and T_{570nm} values between the PMMA samples exposed to methanol for seven days and those of untreated PMMA.

3.3 Effect of flow cell channel width and light slit diameter on chromatographic peak area and efficiency

High detector sensitivity permits analytes to be determined at low concentration levels and requires minimal extra-column band broadening. As peaks broaden, the plate number decreases, indicating reduced separation efficiency [38]. Lower plate numbers result in wider peaks, lower

peak heights, and poorer sensitivity. The effects of channel width and light slit diameter on sensitivity and band broadening were investigated. To identify the optimal channel dimension, widths in the range of 0.8 to 1.2 mm were examined. To carry out these measurements, a mixture of five coumarin dyes at a specific concentration (see experimental section for details) was separated under a constant flow rate and mobile phase composition to eliminate the effect of diffusion coefficient on extra-column band broadening. By increasing the channel width, the linear flow velocity decreased [39] resulting in increased exposure time of the analytes to the excitation source. Therefore, a larger number of molecules within the band were promoted to an excited state resulting in increased fluorescence intensity. As shown in Figure S4, peak areas for all analytes increased by 15% to 35% using a channel width of 1.0 mm. However, decreased linear flow velocity resulted in increased diffusion of analytes from regions of high to low concentration producing band broadening and loss of separation efficiency [39]. It is observed in Figure S4b that increasing the channel width resulted in broader chromatographic peaks. Based on the results, a channel width of 1.0 mm was chosen as optimal in order to reduce extra-column band broadening while achieving acceptable detection sensitivity.

285

286

287

288

289

290

291

292

293

294

295

296

297

298

299

300

301

302

303

304

305

306

307

The material chosen for the slit plate should effectively eliminate most LED light from the slit area. Additionally, the thickness of the slit plate should be minimized to prevent reduction in the intensity of light that reaches the flow cell [40]. Consequently, slit plates with different slit diameters were manufactured by 3D printing using black PLA with a thickness of 1 mm. A series of light slit diameters ranging from 2.5 to 4.0 mm were subsequently studied. As seen in Figure S5a, peak areas increased by 121% to 546% for all dyes using a slit diameter of 3.0 mm, while they increased by only 4% to 32% when a larger slit diameter was used. This is likely due to more light reaching the flow cell at larger slit diameters causing excitation of more fluorescent

molecules; however, a wider pathlength of the flow cell is exposed to the light, resulting in an increased light exposure time of the band and wider chromatographic peaks (Figure S5b). To maintain high chromatographic efficiency and acceptable sensitivity, a slit diameter of 3.5 mm was chosen for the optimum flow cell design.

3.4 Double-channel flow cell geometry to enable detection of co-eluting peaks

308

309

310

311

312

313

314

315

316

317

318

319

320

321

322

323

324

325

326

327

328

329

330

The versatility of the flow cell design enables extension to a double-channel detection system, where bands of analytes simultaneously pass through regions in which LEDs produce different excitation wavelengths. The optimum values for channel width and light slit diameter (vide supra) were used in the design of the flow cell. Coumarin and rhodamine B dyes were chosen to evaluate the performance of the double-channel flow cell since they have different excitation and emission wavelengths. The double-channel flow cell consists of two continuous and connected pathways with the first channel being equipped with a 375 nm LED which lies near the maximum excitation wavelength of coumarin dyes, while the second channel featured a 570 nm LED to detect rhodamine B dye. Three solutions consisting of coumarin and rhodamine B dyes (see experimental for more information) were separated by HPLC and chromatograms for both channels are shown in Figure 4. Separation of four coumarin dyes from the first solution (Figure 4, top row) was achieved with fluorescence being detected only in the first channel. This is due to coumarin dyes absorbing within an excitation range of 250-500 nm and emitting fluorescence between 400-600 nm. In the case of rhodamine B, it appeared in chromatograms from both channels (Figure 4, middle row) since the two LEDs facilitate fluorescence emission. However, the signal from the second channel was of higher intensity than the first due to lower absorption in the first channel. As shown in Figure S6, the maximum absorption wavelength of rhodamine B is near 550 nm. As expected, its signal intensity in the second channel was greater than that of the

first channel, thereby demonstrating the selectivity of this channel. When the third mixture consisting of four coumarin dyes and rhodamine B was chromatographically separated (Figure 4, bottom row), five peaks were detected in channel one and one peak (rhodamine B) was detected in channel two.

The aforementioned results prompted further exploration into the detection of co-eluting peaks and the determination of peak purity. To demonstrate the ability of the double-channel detection strategy to identify and distinguish overlapped peaks in the chromatogram and allow a comparison with a standard UV detector, coumarin 307 was selected and added to the mixture of dyes. Since the retention times of coumarin 307 and rhodamine B are similar, their peaks were overlapped when analyzing the six component mixture. As shown in Figure 5, UV detection was not able to distinguish between coumarin 307 and rhodamine B due to spectral interference. Figure S6 shows that these compounds have continuous absorption throughout the UV range. The chromatogram in the middle panel of Figure 5 (first channel) revealed coumarin 307 and rhodamine B at a retention time of 4.5 min. As expected, the chromatogram from the second channel showed only the rhodamine B peak, permitting its detection without chromatographic interference from coumarin 307. Figure S7 shows the six chromatograms plotted with the R, G, B values using both channels.

3.5 Calibration, sensitivity, and precision

To investigate the figures of merit of the detector in detecting coumarin and rhodamine B dyes, different concentration levels of fluorescent molecules were subjected to HPLC separation and the linear dynamic ranges (LDR), limits of detection (LODs), and limits of quantification (LOQs) measured. Table 1 and Figure 6 show results obtained when varied dye concentrations were subjected to analysis to determine the LDR, slopes of calibration curve, errors of the intercept,

coefficients of determination, and calculated F_{LoF} values. Coefficients of determination higher than 0.991 were obtained for all calibration curves using six different analyte concentration levels injected on the column. Lack of fit test was performed to detect mismatches between the data and the linear equations of the calibration curves generated for each analyte [41]. In this regard, the F_{LoF} values were calculated for all calibration curves, as shown in Table 1, using equation 1,

360
$$F_{LoF} = \frac{\frac{\sum_{i=1}^{n} \sum_{j=1}^{c_{j}} (y_{ij} - b - ax_{i})^{2} - \sum_{i=1}^{n} \sum_{j=1}^{c_{i}} (y_{ij} - \bar{y}_{i})^{2}}{n - 2}}{\frac{\sum_{i=1}^{n} \sum_{j=1}^{c_{i}} (y_{ij} - \bar{y}_{i})^{2}}{(\sum_{i=1}^{n} c_{i}) - n}} [1]$$

where $y_{ij} = ax_i + b$ represents the determined calibration curve equation, n represents the number of measurements, and c indicates the number of measurement replicates [41,42]. By comparing the calculated F_{LoF} values with the critical F value at a significance level of 0.05 (3.26 at $\alpha = 0.05$), $F^{\#}$, it can be concluded that the equations representing the linear calibration curves obtained from this study fit the experimental data.

The LODs and LOQs of each analyte were calculated by reducing the concentration of the analytes until a signal of at least 3.3 and 10 times the average noise level of the detector, respectively, was produced. LODs were observed to range between 0.08 mg L⁻¹ and 0.35 mg L⁻¹ with LOQs ranging from 0.25 mg L⁻¹ to 1.25 mg L⁻¹ for all analytes. The reported figures of merit are highly dependent on different physical and experimental parameters of the separation/detection system, including mobile phase composition, wavelength of excitation source, and light source intensity. Based on previously reported procedures [43,44], intraday and interday precision was calculated by the analysis of standard coumarin dye solutions at three concentration levels (from low, medium and high concentration range from the calibration curve) and the relative standard

deviation (RSD (%)) values determined. Intraday precision was measured by analyzing the results of triplicate injections of standards at different levels in the same day (n = 3). Interday precision was measured from data obtained during a 3-day validation (n = 9). For the intraday study, RSD values were between 1.2 and 5.1% (n = 3) and for the interday study, RSD values were between 1.8 and 7.0% (n = 9), as shown in Table 2. To ascertain whether there is significant differences in the data obtained in three different days, the data were subjected to a one-way analysis of variance (ANOVA) and F-values were calculated, as shown in Table 2. Considering the maximum calculated F-values (4.96) and critical F-value at a significance level of 0.05 (5.14 at $\alpha = 0.05$) taken from the F distribution table, no significant difference in the average of results was observed from three different days. The results demonstrate acceptable repeatability for both intraday and interday precision, as indicated by the RSD values obtained for all the coumarin dyes and one-way ANOVA. In this study, a customized flow cell was employed, which is a consumable component with a cost of approximately \$5 USD. Additionally, the detector introduced in this study is userfriendly, enabling users to effortlessly replace the flow cell in under two minutes if any signal reduction occurs after prolonged usage.

3.6 Analysis of real sample

375

376

377

378

379

380

381

382

383

384

385

386

387

388

389

390

391

392

393

394

395

396

The suitability of the detector for quantifying fluorescent molecules in real samples was investigated, and spiking recoveries were calculated based on previously reported procedures [45,46]. Since the analytes were not detected in the lake and river samples, they were spiked at two concentration levels to assess matrix effects, which can originate from sample components in addition to the analytes that can interfere in quantitative analysis [47]. Figure S8 shows chromatograms of three injections for each spiked level in Lake I water sample. As shown in Table

3, all recoveries were in the range of 91.7–109.7%, with relative standard deviations lower than 6.5%.

A comparison of the HPLC smartphone-based fluorescence detection approach with other fluorescence detectors for the analysis of coumarin dyes and rhodamine B is presented in Table 4. Ping and co-workers reported a LOQ value of 0.016 mg L⁻¹ for rhodamine B using a commercial detector under optimal condition [48]. Ferguson and co-workers reported a rapid acquisition fluorescence detector coupled to HPLC that enabled LODs down to 0.53-1.05 mg L⁻¹ [49], which are comparable to the values obtained in this study.

4. Conclusions

This study reports for the first time the design and construction of a smartphone-based fluorescence detector coupled to HPLC. To reduce fabrication costs and enable miniaturization of the detector, low-cost monochromatic LEDs were used as excitation light sources, and a smartphone camera was used to capture and record the emitted fluorescence in video format. Furthermore, lab-made flow cells were designed to minimize extra-column band broadening and to ensure compatibility with the employed mobile phase composition. A double-channel flow cell geometry was used to identify co-eluting peaks by placing appropriate LEDs within each channel of the flow cell. This study showcases the versatility, sensitivity, and portability of smartphones as detectors for chromatographic separations. When combined with appropriate software tools, smartphones can be used to simultaneously record and process the signal to present chromatograms on the smartphone screen. We envision that this detection approach may help to catalyze the growing trend of chromatographic instrumentation miniaturization by decreasing the costs of necessary components without sacrificing losses in sensitivity. Integration of this detection

approach within the classroom and teaching laboratory may also be beneficial in educating new generations of scientists and engineers about luminescence since the profile of fluorophore-tagged molecules or natively fluorescent molecules can be easily viewed by the user on any smartphone. While numerous advantages of the detector have been highlighted, it is important to acknowledge certain limitations that require improvement in future studies. In the current design, the flow cell is incompatible with acetonitrile and is restricted to mobile phases consisting of methanol and water. Ongoing studies are focused on the development of flow cells based on 3D printing and seek to use acetonitrile-based mobile phases as well as expand the detector's application to include fluorescence molecules with excitation wavelengths lower than 300 nm by incorporating straightforward optical components. Moreover, the current detection method works effectively for detecting fluorescence emission in the visible range. Ongoing efforts are also focused at enhancing this capability by integrating a low-cost and compact electrical component into the smartphone, thereby enabling the detection of ultraviolet light. Additionally, there is currently a lack of a customized smartphone application that would enable users to calculate peak areas and analyze data directly from their smartphones. Furthermore, beyond the optimization of general instrumental parameters discussed in this study, there are several other influential factors that can significantly impact and enhance LOD and LOQ. Among these factors, two parameters of particular importance are the LED emission wavelength and the composition of the mobile phase. It should be noted that since these parameters are highly dependent on the specific analytes under investigation, they were not explored in detail within the scope of this research.

Acknowledgements

420

421

422

423

424

425

426

427

428

429

430

431

432

433

434

435

436

437

438

439

440

441

442

The authors acknowledge funding from the Chemical Measurement and Imaging Program at the National Science Foundation (Grant number CHE-2203891). D.S., S-A.H., and J.L.A. thank

the Alice Hudson Professorship at Iowa State University for support. I.O-R. acknowledges the U.S.-Mexico Commission for Educational and Cultural Exchange (COMEXUS) for the Fulbright García-Robles Visiting Scholar Award. Victoria Zeger is thanked for assisting in statistical analyses performed throughout this work.

References

466

467 [1] J.W. Dolan, How Does It Work? Part V: Fluorescence Detectors, LCGC N. Am. 34 (2016) 710–719. 468 469 [2] E. Lipka, C. Vaccher, Quantitative analysis of drugs in biological matrices by HPLC 470 471 hyphenated to fluorescence detection, Bioanalysis. 7 (2015) 743–762. 472 https://doi.org/10.4155/bio.15.20. 473 [3] M. Kai, Y. Ohkura, Fluorescence derivatization of bioactive peptides for high-performance 474 475 liquid chromatography, TrAC Trends Anal. Chem. 6 (1987) 116–120. https://doi.org/10.1016/0165-9936(87)87053-X. 476 477 [4] C.-M. Chen, J.-A. Lee, T.-C. Huang, Construction of a light-emitting diode fluorescence 478 detector for high-performance liquid chromatography and its application to fluorometric 479 determination of 1-3-hydroxybutyrate, Biomed. Chromatogr. 26 (2012) 256–260. 480 481 https://doi.org/10.1002/bmc.1655. 482 [5] F. Dang, X. Geng, J. Li, J. Wang, Y. Guan, A miniaturized and high sensitive dual channel 483 fluorimeter based on compact collinear optical arrangement, Talanta. 211 (2020) 120698. 484 https://doi.org/10.1016/j.talanta.2019.120698. 485 486 [6] S. Chatzimichail, F. Rahimi, A. Saifuddin, A.J. Surman, S.D. Taylor-Robinson, A. Salehi-487 Reyhani, Hand-portable HPLC with broadband spectral detection enables analysis of 488

- complex polycyclic aromatic hydrocarbon mixtures, Commun. Chem. 4 (2021) 1–14. 489 https://doi.org/10.1038/s42004-021-00457-7. 490 491 492 [7] B. Chouhan, P.K. Dasgupta, Direct Photothermal Measurement of Optical Absorption in a Flow System, Anal. Chem. 91 (2019) 2923–2931. 493 https://doi.org/10.1021/acs.analchem.8b05091. 494 495 496 [8] S. Sharma, H.D. Tolley, P.B. Farnsworth, M.L. Lee, LED-Based UV Absorption Detector with Low Detection Limits for Capillary Liquid Chromatography, Anal. Chem. 87 (2015) 497 1381–1386. https://doi.org/10.1021/ac504275m. 498 499 500 [9] S.W. Foster, M.J. Alirangues, J.A. Naese, E. Constans, J.P. Grinias, A low-cost, open-source digital stripchart recorder for chromatographic detectors using a Raspberry Pi, J. 501 502 Chromatogr. A. 1603 (2019) 396–400. https://doi.org/10.1016/j.chroma.2019.03.070. 503 [10] A. Ishida, M. Fujii, T. Fujimoto, S. Sasaki, I. Yanagisawa, H. Tani, M. Tokeshi, A 504
- 508
 509 [11] W. Wongwilai, S. Lapanantnoppakhun, S. Grudpan, K. Grudpan, Webcam camera as a
 510 detector for a simple lab-on-chip time based approach, Talanta. 81 (2010) 1137–1141.

1163–1169. https://doi.org/10.2116/analsci.31.1163.

https://doi.org/10.1016/j.talanta.2010.01.058.

505

506

507

511

Portable Liquid Chromatograph with a Battery-operated Compact Electroosmotic Pump and

a Microfluidic Chip Device with a Reversed Phase Packed Column, Anal. Sci. 31 (2015)

- E. da N. Gaiao, V.L. Martins, W. da S. Lyra, L.F. de Almeida, E.C. da Silva, M.C.U. 512 [12] Araújo, Digital image-based titrations, Anal. Chim. Acta. 570 (2006) 283–290. 513 514 https://doi.org/10.1016/j.aca.2006.04.048. 515 M.V. Gorbunova, A.S. Safronova, A.A. Vasilyeva, K.S. Spitsyna, V.V. Apyari, S.G. 516 [13] Dmitrienko, Sulfonamide drugs: Low-cost spectrofluorometric determination using a 517 computer monitor calibrator for detection, Talanta. 257 (2023) 124383. 518 https://doi.org/10.1016/j.talanta.2023.124383. 519 520 V.V. Apyari, S.G. Dmitrienko, Y.A. Zolotov, Unusual application of common digital 521 [14] 522 devices: Potentialities of Eye-One Pro mini-spectrophotometer – A monitor calibrator for 523 registration of surface plasmon resonance bands of silver and gold nanoparticles in solid matrices, Sens. Actuators B Chem. 188 (2013) 1109–1115. 524 525 https://doi.org/10.1016/j.snb.2013.07.097. 526 [15] L. Zhu, S. Yang, Z. Xiao, H. Huang, K. Yan, S. Wang, A portable Raspberry Pi-based 527 spectrometer for on-site spectral testing, Anal. Methods. 15 (2023) 3092–3100. 528 https://doi.org/10.1039/d3ay00464c. 529
- [16] J.J.K. Chng, M.Y. Patuwo, Building a Raspberry Pi Spectrophotometer for
 Undergraduate Chemistry Classes, J. Chem. Educ. 98 (2021) 682–688.
 https://doi.org/10.1021/acs.jchemed.0c00987.

- A. Bogomolova, M. Aldissi, Real-time aptamer quantum dot fluorescent flow sensor, 535 [17] Biosens. Bioelectron. 26 (2011) 4099–4103. https://doi.org/10.1016/j.bios.2011.04.001. 536 537 [18] Z. Liu, Y. Zhang, S. Xu, H. Zhang, Y. Tan, C. Ma, R. Song, L. Jiang, C. Yi, A 3D printed 538 smartphone optosensing platform for point-of-need food safety inspection, Anal. Chim. Acta. 539 966 (2017) 81–89. https://doi.org/10.1016/j.aca.2017.02.022. 540 541 542 [19] C.-K. Choi, S.M. Shaban, B.-S. Moon, D.-G. Pyun, D.-H. Kim, Smartphone-assisted point-of-care colorimetric biosensor for the detection of urea via pH-mediated AgNPs 543 growth, Anal. Chim. Acta. 1170 (2021) 338630. https://doi.org/10.1016/j.aca.2021.338630. 544 545 546 [20] M. Rezazadeh, S. Seidi, M. Lid, S. Pedersen-Bjergaard, Y. Yamini, The modern role of smartphones in analytical chemistry, TrAC Trends Anal. Chem. 118 (2019) 548–555. 547 https://doi.org/10.1016/j.trac.2019.06.019. 548 549 X. Ding, M.G. Mauk, K. Yin, K. Kadimisetty, C. Liu, Interfacing Pathogen Detection 550 [21] with Smartphones for Point-of-Care Applications, Anal. Chem. 91 (2019) 655–672. 551 https://doi.org/10.1021/acs.analchem.8b04973. 552 553 W. Chen, Y. Yao, T. Chen, W. Shen, S. Tang, H.K. Lee, Application of smartphone-554 [22]
- based spectroscopy to biosample analysis: A review, Biosens. Bioelectron. 172 (2021)

 112788. https://doi.org/10.1016/j.bios.2020.112788.

T. Beduk, D. Beduk, M.R. Hasan, E. Guler Celik, J. Kosel, J. Narang, K.N. Salama, S. 557 [23] Timur, Smartphone-Based Multiplexed Biosensing Tools for Health Monitoring, Biosensors. 558 559 12 (2022) 583. https://doi.org/10.3390/bios12080583. 560 S.-A. Hsieh, D. Shamsaei, D.R. Eitzmann, J.L. Anderson, Digital Droplet Loop-Mediated [24] 561 Isothermal Amplification Featuring a Molecular Beacon Assay, 3D Printed Droplet 562 Generation, and Smartphone Imaging for Sequence-Specific DNA Detection, Anal. Chem. 563 94 (2022) 11949–11956. https://doi.org/10.1021/acs.analchem.2c02979. 564 565 W. Yu, C. Jiang, B. Xie, S. Wang, X. Yu, K. Wen, J. Lin, J. Wang, Z. Wang, J. Shen, 566 [25] 567 Ratiometric fluorescent sensing system for drug residue analysis: Highly sensitive 568 immunosensor using dual-emission quantum dots hybrid and compact smartphone baseddevice, Anal. Chim. Acta. 1102 (2020) 91–98. https://doi.org/10.1016/j.aca.2019.12.037. 569 570 [26] D.R. Eitzmann, D. Shamsaei, J.L. Anderson, Versatile dual-channel loop-mediated 571 isothermal amplification assay featuring smartphone imaging enables determination of fecal 572 indicator bacteria in environmental waters, Talanta. 265 (2023) 124890. 573 https://doi.org/10.1016/j.talanta.2023.124890. 574 575 Y. Zhang, T. Xue, L. Cheng, J. Wang, R. Shen, J. Zhang, Smartphone-assisted 576 [27] colorimetric biosensor for on-site detection of Cr3+ ion analysis, Anal. Chim. Acta. 1199 577

(2022) 339603. https://doi.org/10.1016/j.aca.2022.339603.

A. Shahvar, M. Saraji, D. Shamsaei, Headspace single drop microextraction combined 579 [28] with mobile phone-based on-drop sensing for the determination of formaldehyde, Sens. 580 581 Actuators B Chem. 273 (2018) 1474–1478. https://doi.org/10.1016/j.snb.2018.07.071. 582 [29] S. Tang, T. Qi, D. Xia, M. Xu, M. Xu, A. Zhu, W. Shen, H.K. Lee, Smartphone 583 Nanocolorimetric Determination of Hydrogen Sulfide in Biosamples after Silver-Gold 584 Core-Shell Nanoprism-Based Headspace Single-Drop Microextraction, Anal. Chem. 91 585 (2019) 5888–5895. https://doi.org/10.1021/acs.analchem.9b00255. 586 587 A. Shahvar, M. Saraji, D. Shamsaei, Smartphone-based chemiluminescence sensing for 588 [30] 589 TLC imaging, Sens. Actuators B Chem. 255 (2018) 891–894. 590 https://doi.org/10.1016/j.snb.2017.08.144. 591 M. Zangheri, F. Di Nardo, D. Calabria, E. Marchegiani, L. Anfossi, M. Guardigli, M. 592 [31] 593 Mirasoli, C. Baggiani, A. Roda, Smartphone biosensor for point-of-need chemiluminescence detection of ochratoxin A in wine and coffee, Anal. Chim. Acta. 1163 (2021) 338515. 594 https://doi.org/10.1016/j.aca.2021.338515. 595 596 P.M. Kalligosfyri, A. Sevastou, I.K. Kyriakou, S.S. Tragoulias, D.P. Kalogianni, T.K. [32] 597 Christopoulos, Smartphone-based chemiluminometric hybridization assays and quantitative 598 competitive polymerase chain reaction, Anal. Chim. Acta. 1088 (2019) 123–130. 599 https://doi.org/10.1016/j.aca.2019.08.051. 600

Based Electrochemiluminescence for Visual Simultaneous Detection of RASSF1A and 603 604 SLC5A8 Tumor Suppressor Gene Methylation in Thyroid Cancer Patient Plasma, Anal. Chem. 94 (2022) 8005–8013. https://doi.org/10.1021/acs.analchem.2c01132. 605 606 [34] V.D. Nguyen, H.Q. Nguyen, K.H. Bui, Y.S. Ko, B.J. Park, T.S. Seo, A handheld-type 607 total integrated capillary electrophoresis system for SARS-CoV-2 diagnostics: Power, 608 fluorescence detection, and data analysis by smartphone, Biosens. Bioelectron. 195 (2022) 609 113632. https://doi.org/10.1016/j.bios.2021.113632. 610 611 [35] R. Zenhausern, A.S. Day, B. Safavinia, S. Han, P.E. Rudy, Y.-W. Won, J.-Y. Yoon, 612 613 Natural killer cell detection, quantification, and subpopulation identification on paper microfluidic cell chromatography using smartphone-based machine learning classification, 614 615 Biosens. Bioelectron. 200 (2022) 113916. https://doi.org/10.1016/j.bios.2021.113916. 616 [36] M.M. Ibrahim, K.M. Kelani, N.K. Ramadan, E.S. Elzanfaly, Smartphone as a Portable 617 Detector for Thin-Layer Chromatographic Determination of Some Gastrointestinal Tract 618 Drugs, ACS Omega. 7 (2022) 23815–23820. https://doi.org/10.1021/acsomega.2c02482. 619 620 [37] D. Parriott, A Practical Guide to HPLC Detection, Academic Press, 2012. 621 622 623 [38] Snyder, L.R., Kirkland, J.J. and Dolan, J.W. (2009). Frontmatter. In Introduction to Modern Liquid Chromatography (eds L.R. Snyder, J.J. Kirkland and J.W. Dolan). 624 https://doi.org/10.1002/9780470508183.fmatter 625

S.M. Khoshfetrat, P. Seyed Dorraji, M. Shayan, F. Khatami, K. Omidfar, Smartphone-

602

[33]

T. Werres, T.C. Schmidt, T. Teutenberg, Peak broadening caused by using different 626 [39] micro-liquid chromatography detectors, Anal. Bioanal. Chem. 414 (2022) 6107–6114. 627 628 https://doi.org/10.1007/s00216-022-04170-9. 629 [40] X. Geng, D. Wu, Y. Guan, A compact and highly sensitive light-emitting diode-induced 630 fluorescence detector for capillary flow systems, Talanta. 88 (2012) 463-467. 631 https://doi.org/10.1016/j.talanta.2011.11.015. 632 633 R.I. Rawski, P.T. Sanecki, K.M. Kijowska, P.M. Skitat, D.E. Saletnik, Regression 634 [41] analysis in analytical chemistry. Determination and validation of linear and quadratic 635 regression dependencies, South Afr. J. Chem. 69 (2016) 166–173. 636 637 D.L Massart, B.G.M. Vandeginste, L.M.C. Buydens, S. De Jong, P.J. Lewi, J. Smeyers-[42] 638 Verbeke, Handbook of Chemometrics and Qualimetrics: Part A, Elsevier, 1997. 639 640 [43] Simultaneous determination of prednisolone, prednisolone acetate and hydrocortisone in 641 human serum by high-performance liquid chromatography, J. Chromatogr. B. Biomed. Sci. 642 App. 674 (1995) 237–246. https://doi.org/10.1016/0378-4347(95)00317-7. 643 644 W. Zeng, D.G. Musson, A.L. Fisher, L. Chen, M.S. Schwartz, E.J. Woolf, A.Q. Wang, [44] 645 Determination of sitagliptin in human urine and hemodialysate using turbulent flow online 646

extraction and tandem mass spectrometry, J. Pharm. Biomed. Anal. 46 (2008) 534–542.

https://doi.org/10.1016/j.jpba.2007.11.003.

647

Y. Cao, Y. Liu, F. Li, S. Guo, Y. Shui, H. Xue, L. Wang, Portable colorimetric detection 649 [45] of copper ion in drinking water via red beet pigment and smartphone, Microchem. J. 150 650 651 (2019) 104176. https://doi.org/10.1016/j.microc.2019.104176. 652 A. Shahvar, D. Shamsaei, M. Saraji, A portable smartphone-based colorimetric sensor for [46] 653 rapid determination of water content in ethanol, Measurement. 150 (2020) 107068. 654 https://doi.org/10.1016/j.measurement.2019.107068. 655 656 G.G. Guilbault, M. Hjelm, Nomenclature for automated and mechanised analysis 657 [47] (Recommendations 1989), Pure Appl. Chem. 61 (1989) 1657–1664. 658 659 https://doi.org/10.1351/pac198961091657. 660 [48] W. Ping, X. Zhu, B. Wang, An Ionic Liquid Loaded β-Cyclodextrin-Cross-Linked 661 Polymer as the Solid Phase Extraction Material Coupled with High-Performance Liquid 662 Chromatography for the Determination of Rhodamine B in Food, Anal. Lett. 47 (2014) 504– 663 516. https://doi.org/10.1080/00032719.2013.841177. 664 665 T. Ferguson, A. Bernicky, I. Kozin, H.-P. Loock, HPLC-Detector Based on Hadamard-666 [49] Transform Fluorescence Excitation-Emission-Matrix Spectroscopy, Anal. Chem. 93 (2021) 667 8116–8121. https://doi.org/10.1021/acs.analchem.1c01037. 668 669 670 671

Table 1. Analytical performance of the smartphone-based detector in the determination of six coumarin and rhodamine B dyes. The dyes were detected using LEDs with maximum wavelengths of 375 and 570 nm, respectively. Calibration curves of rhodamine B were plotted using the peak area of the R value from the chromatogram in the separation of six different concentration levels of rhodamine B on the column. Calibration curves of coumarin 466 and coumarin 307 were plotted using the peak area of B values while coumarin 307, coumarin 153, and coumarin 6 were plotted using the peak area of G values from the separation of mixtures consisting of five coumarin dyes. All calibration curves were performed in triplicate.

Analytes	Limit of Detection (mg L ⁻¹)	Limit of Quantitation (mg L ⁻¹)	Linear Dynamic Range (mg L ⁻¹)	Coefficient of Determination (R ²)	Slope ± SD	Intercept ± SD	$F_{LoF}{}^{ m a}$
Coumarin 120	0.08	0.25	0.25-2.50	0.994	645.1±12.4	-120.9±18.1	0.87
Coumarin 466	0.08	0.25	0.25-2.50	0.995	486.4±8.7	-81.7±12.8	0.32
Coumarin 307	0.08	0.25	0.25-2.50	0.995	650.2±11.4	74.0±16.7	2.57
Coumarin 153	0.30	1.00	1.00-10.00	0.991	216.3±5.2	130.9±29.4	2.80
Coumarin 6	0.35	1.25	1.25-12.50	0.991	222.7±5.4	123.6±38.0	3.17
Rhodamine B	0.35	1.25	1.25-20.00	0.995	174.6±3.2	-58.7±31.9	2.86

^a Represents the calculated F value for Lake of Fit test using equation 1.

Table 2. Intraday and interday precision for the determination of coumarin dyes in standard solutions using the smartphone-based fluorescence detector.

	Concentration level I					Concentration level II					Concentration level III				
	RSD (%)		Interday precision RSD (%)	F value ^a	Intraday precision RSD (%)		Interday precision RSD (%)	F value ^a	RSD (%)		Interday precision RSD (%)	F value ^a			
Analytes	Day 1	Day 2	Day 3			Day 1	Day 2	Day 3			Day 1	Day 2	Day 3		
Coumarin 120	4.3	2.9	4.1	4.4	1.18	2.0	1.9	2.9	2.9	3.84	5.1	5.0	4.4	7.0	4.86
Coumarin 466	3.5	4.8	3.9	5.5	3.24	2.2	1.3	3.8	2.8	1.71	2.1	1.3	1.5	1.8	1.51
Coumarin 307	3.0	4.4	4.7	6.1	4.96	4.2	2.4	4.3	3.3	3.10	4.6	4.5	3.7	4.5	1.40
Coumarin 153	4.0	4.0	5.1	4.3	0.95	2.6	4.0	5.1	3.5	2.99	3.3	3.7	4.1	3.4	0.44
Coumarin 6	2.8	1.8	5.0	3.1	2.28	4.7	1.2	2.9	2.7	1.04	5.3	3.1	3.3	4.2	1.18
684															

Concentration level I: 0.50, 0.50, 0.50, 2.00, and 2.50 mg L^{-1} for coumarin 120, coumarin 466, coumarin 307, coumarin 153 and coumarin 6, respectively. Concentration level II: 1.00, 1.00, 1.00, 4.00, and 5.00 mg L^{-1} for coumarin 120, coumarin 466, coumarin 307, coumarin 153 and coumarin 6, respectively. Concentration level III: 2.00, 2.00, 2.00, 8.00, and 10.00 mg L^{-1} for coumarin 120, coumarin 466, coumarin 307, coumarin 153 and coumarin 6, respectively.

^a Represents the calculated F value in one-way ANOVA.

691

692

693

694

695

696

Concentration of spiked analytes at level I: 0.60, 0.40, 0.40, 1.25, and 1.60 mg L^{-1} for coumarin 120, coumarin 466, coumarin 307, coumarin 153 and coumarin 6, respectively.

Concentration of spiked analytes at level II: 1.50, 1.00, 1.00, 3.10, and 4.00 mg L^{-1} for coumarin 120, coumarin 466, coumarin 307, coumarin 153 and coumarin 6, respectively.

^a Spiking recovery.
^b Relative standard deviation.

Table 4. Comparison of the smartphone-based fluorescence detector with other reported methods from the literature for the determination of coumarin and rhodamine B dyes.

Methodology	Analytes	L^{-1}) L^{-1}) d		Linear dynamic range (mg L ⁻¹)	Reference
HPLC/FD ^d	Rhodamine B	0.002	0.016	0.016-2.600	[48]
HPLC/HT-EEM/e	Coumarin 440	0.53	1.75	NR°	[49]
	Coumarin 450	0.85	2.40		
	Coumarin 307	1.05	3.30		
	Coumarin 460	0.90	3.00		
	Coumarin 540A	0.60	1.90		
HPLC/SBFD ^f	Coumarin 120	0.08	0.25	0.25-2.50	Present study
	Coumarin 466	0.08	0.25	0.25-2.50	
	Coumarin 307	0.08	0.25	0.25-2.50	
	Coumarin 153	0.30	1.00	1.00-10.00	
	Coumarin 6	0.35	1.25	1.25-12.50	
	Rhodamine B	0.35	1.25	1.25-20.00	

⁷⁴¹

^{742 &}lt;sup>a</sup> Limit of detection.

^{743 &}lt;sup>b</sup> Limit of quantitation.

^{744 °} Not reported.

⁷⁴⁵ dHPLC coupled to fluorescence detection.

^e Hadamard-Transform fluorescence excitation-emission-matrix spectroscopy.

⁷⁴⁷ f Smartphone-based fluorescence detector.

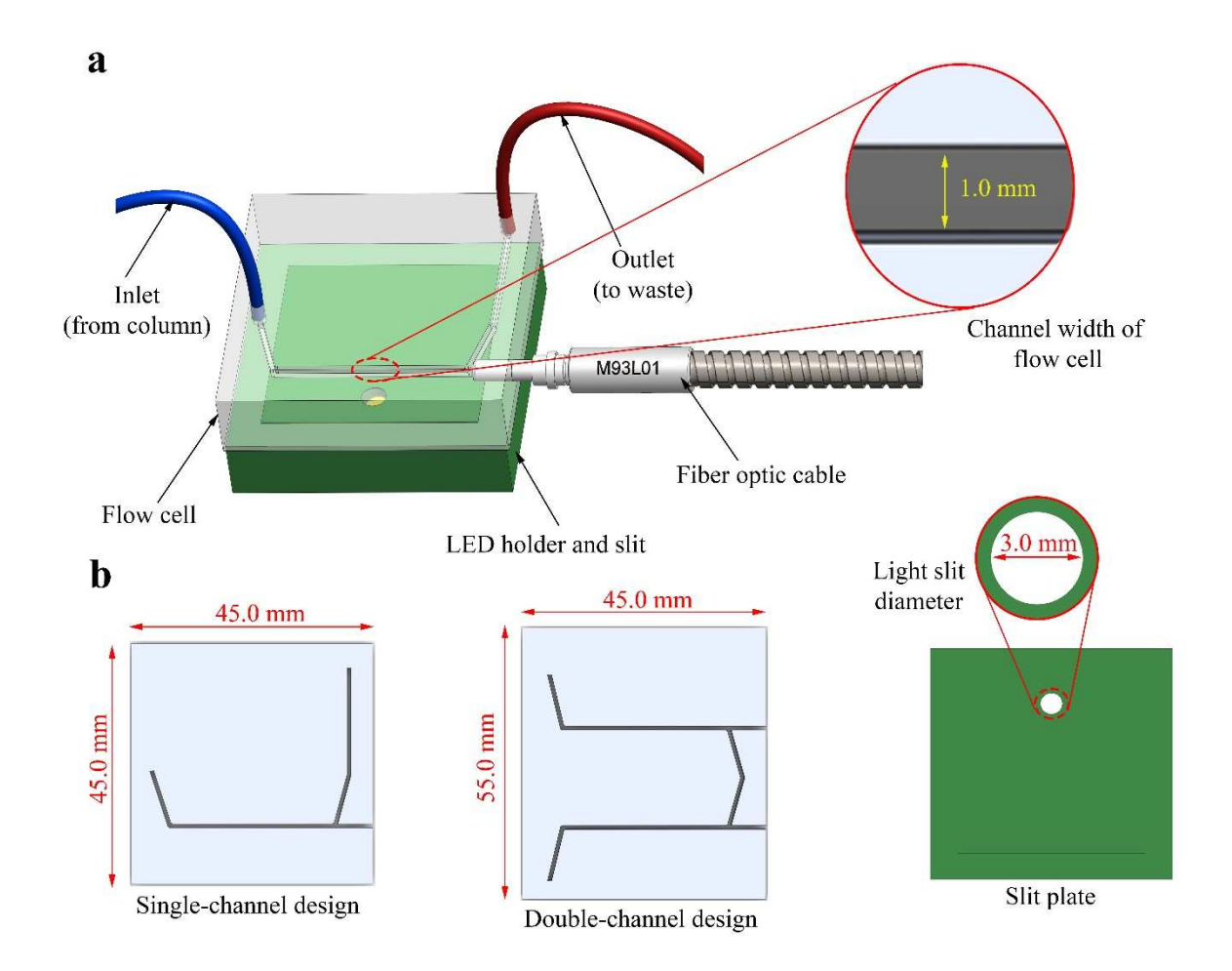


Figure 1. (a) Three-dimensional schematic of the assembled single-channel flow cell showing all components and featuring a channel width of 1.0 mm. (b) Schematic of the single-channel design (left), double-channel design (middle) and slit plate with a slit diameter of 3.0 mm (right).

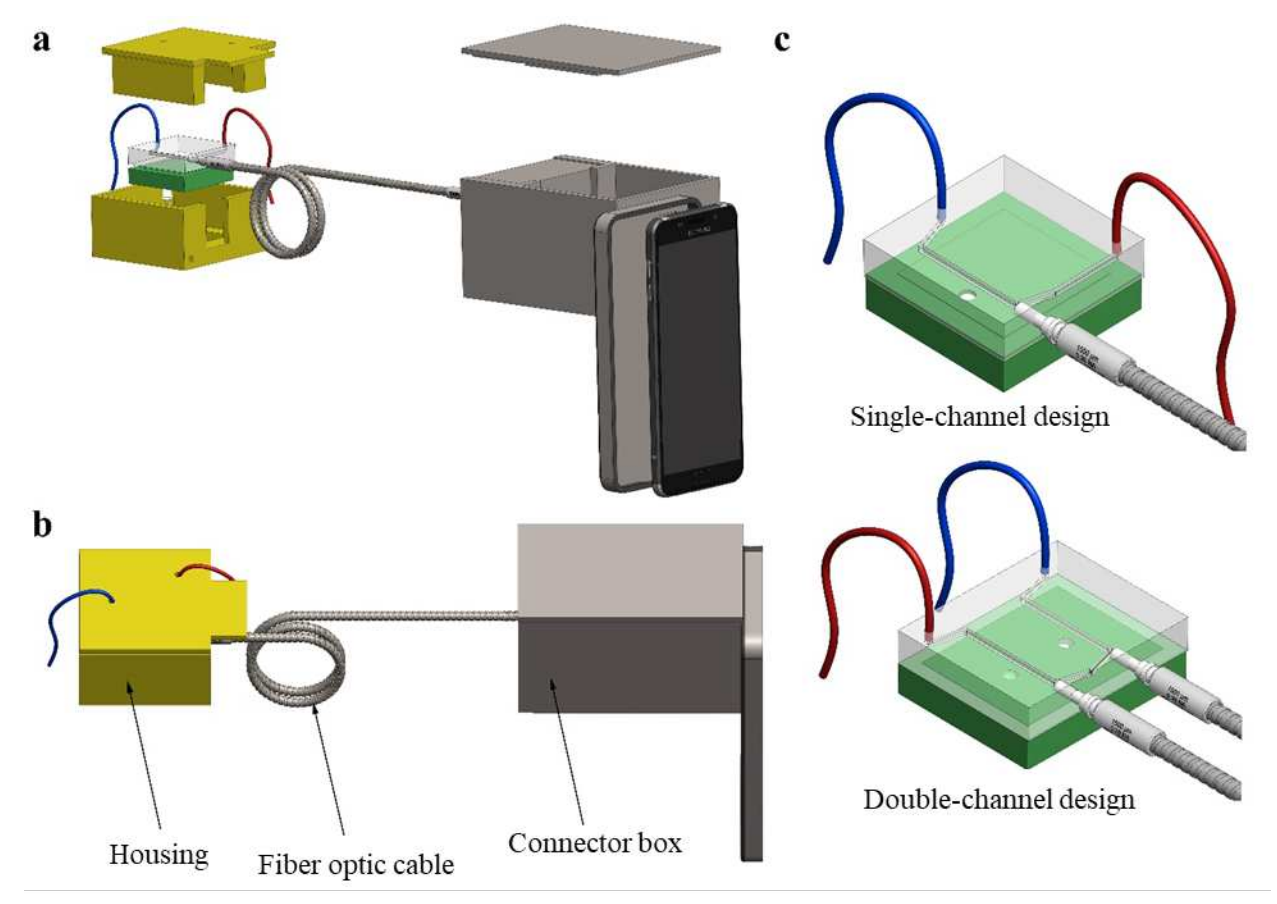


Figure 2. Components and their assembly to form the complete smartphone-based fluorescence detector developed in this study. (a) Schematic showing the housing, single-channel flow cell, PEEK tubing, LED holder, LED, fiber optic cable, connector box, and smartphone. (b) Side view of the assembled system. (c) Three-dimensional schematic of assembled single and double-channel flow cells prepared by CNC milling using clear PMMA. The single-channel flow cell is comprised of a fiber optic cable and a monochromatic LED. The double-channel flow cell is comprised of two fiber optic cables and two monochromatic LEDs. Each fiber optic cable is used for transferring emitted light from the flow cell to the connector box for smartphone imaging.

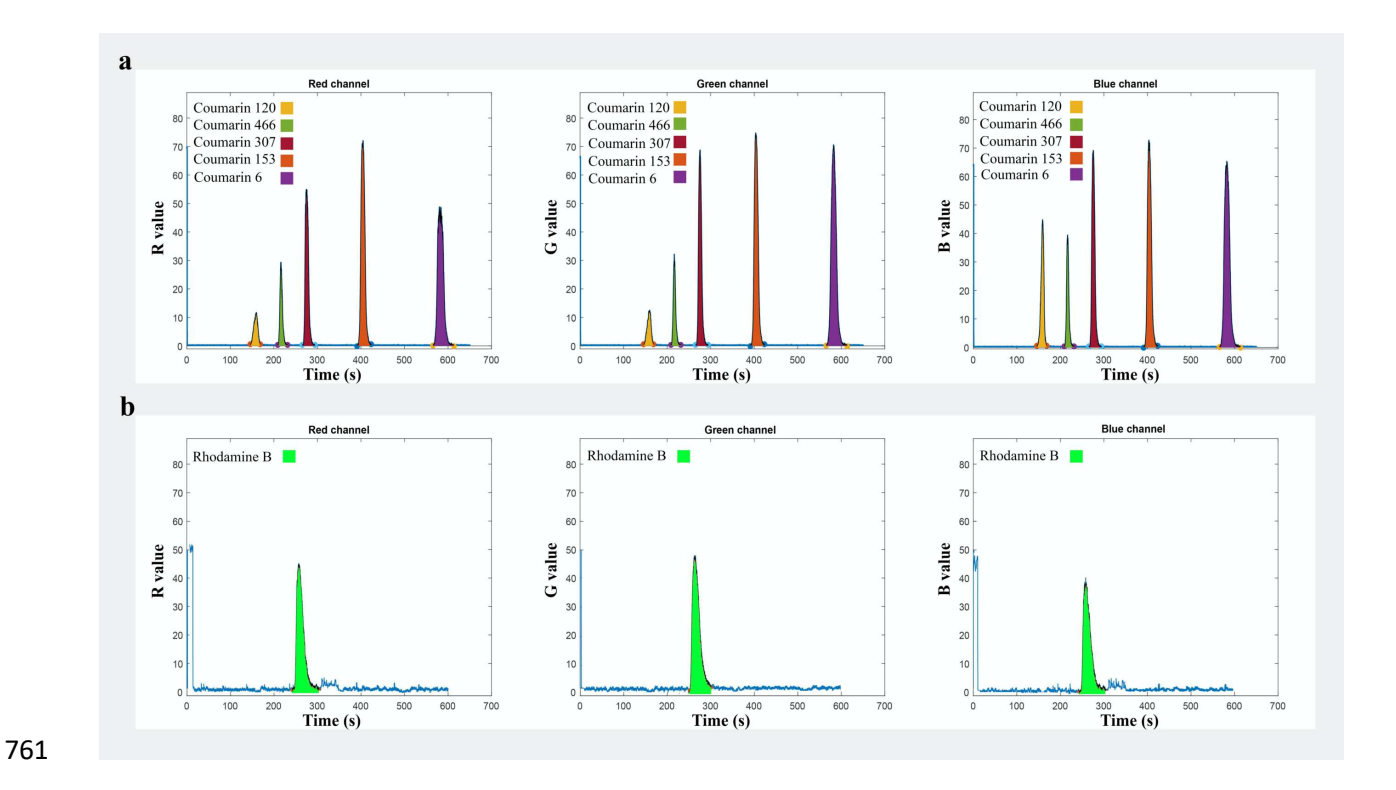


Figure 3. Chromatograms plotted by MATLAB after image processing showing the separation of coumarin and rhodamine B dyes using the smartphone-based fluorescence detector. (a) Chromatograms of red (left), green (middle) and blue (right) channels resulting from the separation of a mixture consisting of coumarin 120 (0.6 mg L⁻¹), coumarin 466 (0.6 mg L⁻¹), coumarin 307 (0.6 mg L⁻¹), coumarin 153 (2.5 mg L⁻¹), and coumarin 6 (3.1 mg L⁻¹) dyes. The analytes were detected by a LED offering a maximum wavelength of 375 nm. (b) Chromatograms of red (left), green (middle) and blue (right) channels in the separation of rhodamine B (5.0 mg L⁻¹). A LED with a maximum wavelength of 570 nm was used. A flow cell width and slit diameter of 1.0 mm and 3.0 mm, respectively, were used for separations carried out in (a) and (b).

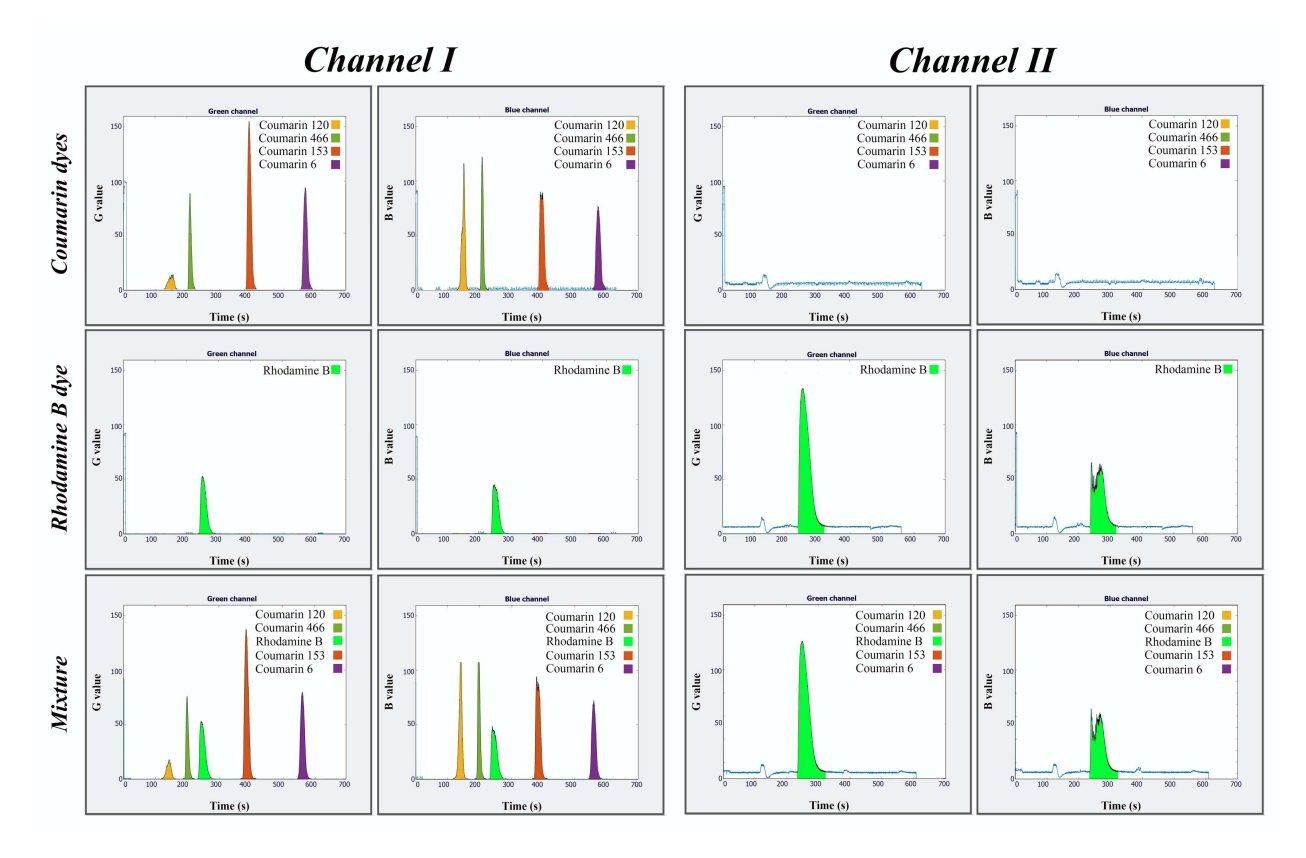


Figure 4. Chromatograms showing the separation of coumarin and rhodamine B dyes from three different dye solutions using the double-channel flow cell design. Each row is the result of analyzing both channels from a single HPLC run. Channel I is equipped with a 375 nm LED and channel II employs a 570 nm LED. The top row is the separation from a mixture consisting of coumarin 120, coumarin 466, coumarin 153 and coumarin 6. In the middle row, rhodamine B was subjected to separation and appeared in the chromatograms of both channels; however, the signal intensity in the second channel is higher than the first channel. The bottom row shows the separation of a mixture consisting of coumarin 120, coumarin 466, coumarin 153, coumarin 6 and rhodamine B dyes. All analytes were detected within the first channel; however, only rhodamine B was detected in channel II.

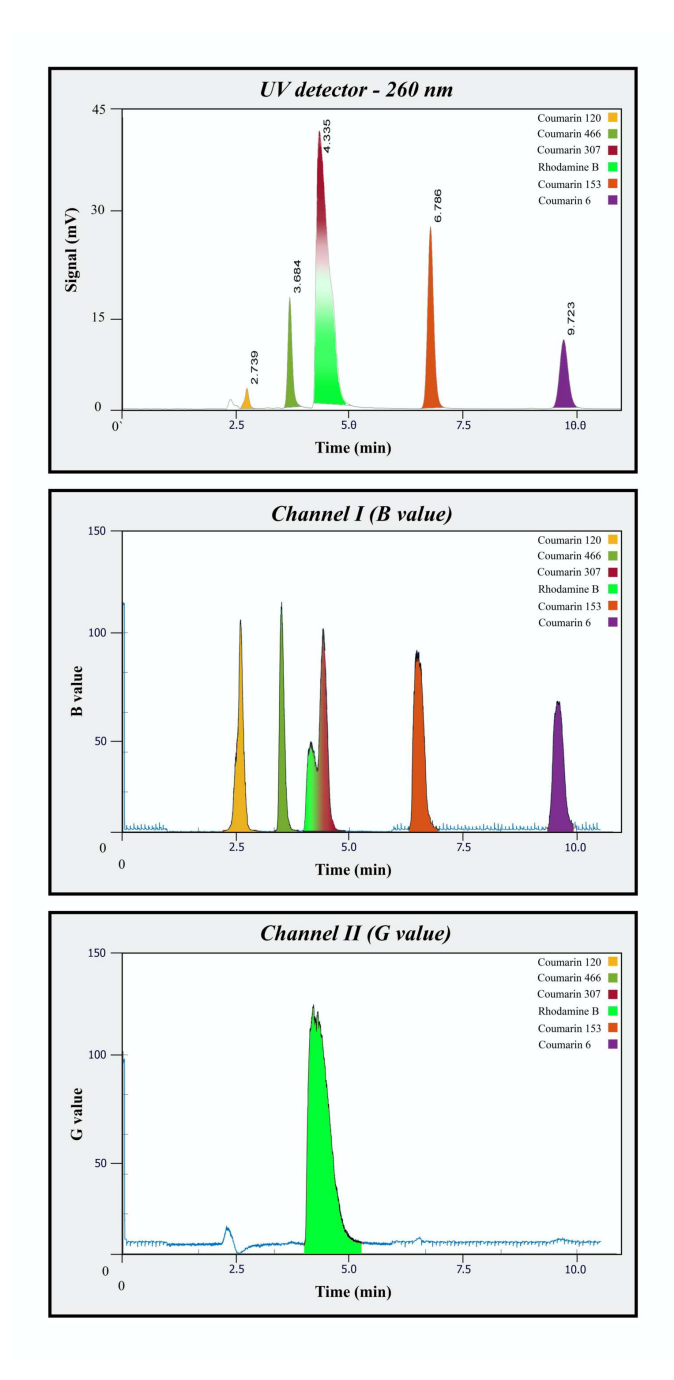


Figure 5. (Top) Chromatogram obtained from the separation of coumarin 120, coumarin 466, coumarin 307, coumarin 153, coumarin 6 and rhodamine B using a UV/vis detector set at a detection wavelength of 260 nm. The chromatogram shows the limitation of UV/vis detection in identifying and separating the co-elution of coumarin 307 and rhodamine B. (Middle and Bottom)) Chromatograms obtained from the separation of coumarin 120, coumarin 466, coumarin 307, coumarin 153, coumarin 6 and rhodamine B using a double-channel flow cell geometry and smartphone-based fluorescence detection. The chromatogram in the middle panel shows channel I and the bottom panel shows channel II. Channel I is equipped with 375 nm LED and channel II employs a 570 nm LED.

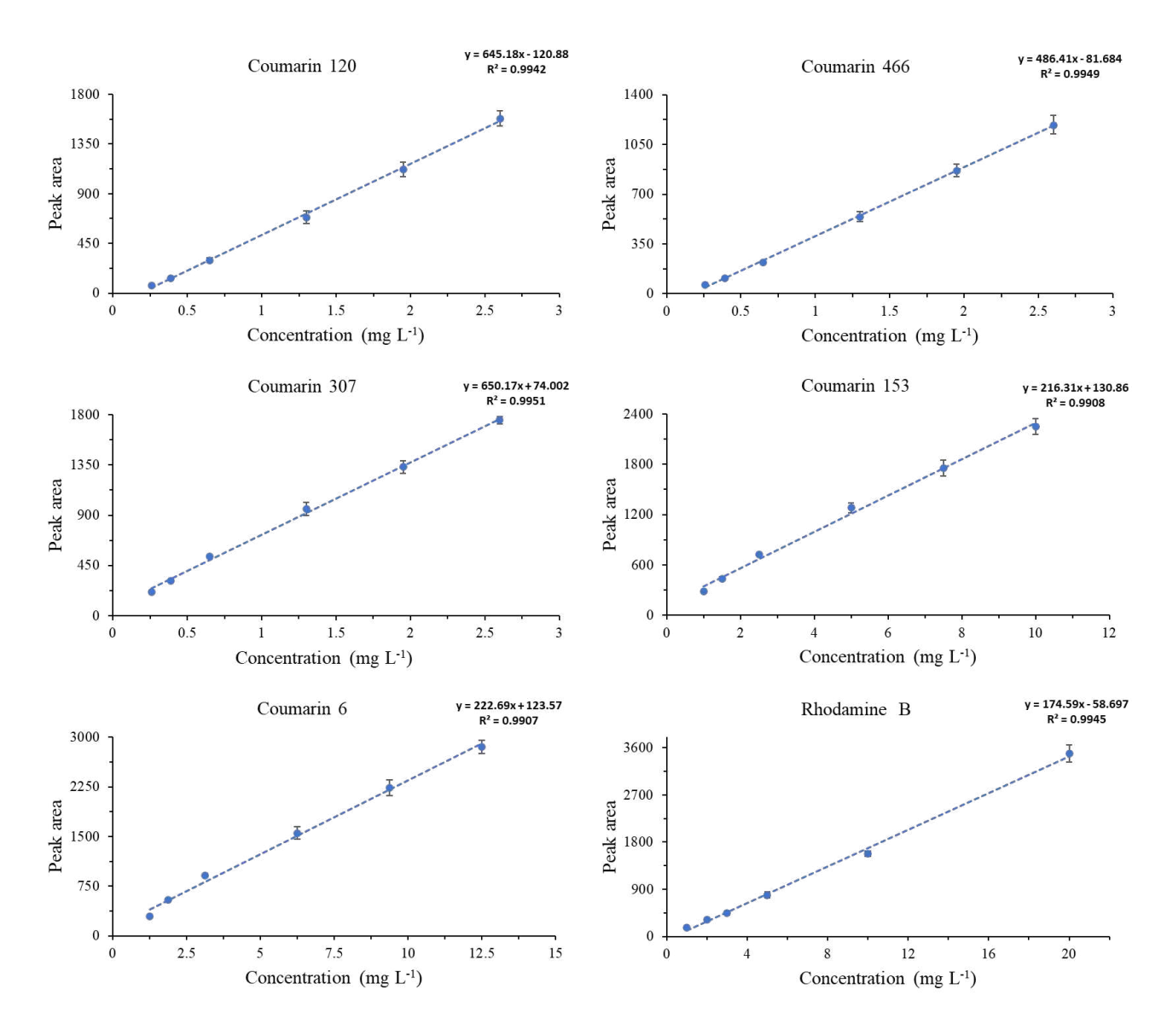


Figure 6. Six-point calibration curves constructed for each of the six dyes evaluated in this study using the smartphone-based fluorescence detector. The concentration of analytes subjected to chromatographic separation are given on the x-axis while peak areas are shown on the y-axis. Coumarin dyes were detected by a LED offering a maximum wavelength of 375 nm while rhodamine B was detected by a LED offering a maximum wavelength of 570 nm. To construct the calibration curves, the R value was used for the peak area of rhodamine B, the B values were used for peak areas of coumarin 120 and coumarin 466, and the G values were used for peak areas of coumarin 153 and coumarin 6 dyes. All measurements were performed in triplicate.